PCCP

Accepted Manuscript

ROYAL SOCIETY OF CHEMISTRY

www.rsc.org/pccp

Excluded volume effects on ionic partitioning in gels and microgels: A simulation study

Silvia Ahualli,[a] Alberto Martín-Molina,[b] and Manuel Quesada-Pérez[a]

a) Departamento de Física, Escuela Politécnica Superior de Linares, Universidad de Jaén, 23700, Linares, Jaén, Spain.

b) Grupo de Física de Fluidos y Biocoloides, Departamento de Física Aplicada, Facultad de Ciencias, Universidad de Granada, 18071 Granada, Spain.

ABSTRACT.

In this work the effect of volume exclusion on ionic partitioning in swollen and moderately collapsed gels has been studied through coarse-grained simulations. Our results show that finite size effects yield deviations from the classical theory of Donnan exclusion. At low or moderate reservoir electrolyte concentration these discrepancies become important if one of the ions has diameters of just a few nanometers. When the reservoir electrolyte concentration grows, volume exclusion can lead to a drastic failure of the ideal Donnan exclusion even for conventional hydrated monoatomic ions. In addition, an approximate analytical expression for the partition coefficient of ionic species including the volume exclusion associated to the polymer network and the neutralizing counterions has been proposed and tested. This theoretical approach also provides an expression for the Donnan potential difference that takes such effects into account. Good agreement between theory and simulations is found for slightly and moderately charged gels (both at low and high reservoir electrolyte concentrations). The theory also works acceptably for highly charged gels at high salt concentrations or for electrolytes with large counterions.

INTRODUCTION.

Certain polymers and polyelectrolytes can be synthesized forming cross-linked networks usually known as gels, microgels or even nanogels, depending on the size of the network. One of the most intriguing properties of hydrogels and their submicron counterparts is their ability to uptake and release aqueous solutes in a controlled fashion since they can absorb large amounts of water in response to changes in some environmental conditions, such as temperature and/or pH.[1,2] The equilibrium ratio of the solute concentration in a porous material to that in bulk solution, known as the partition coefficient, plays a key role innumerous separation processes (such as chromatography ultrafiltration or gel electrophoresis) in which gels are involved. It is also an important quantity in some biomedical applications of these smart materials, such as the controlled uptake and release of pharmaceuticals.[3] In addition, there is a direct interplay between the partitioning of a given electrolyte into a gel and its swelling behavior in the presence of salt.

The quantity of solute into a gel clearly depends on the different interactions between the polymer network and the solute. In the case of neutral solutes and absent specific interactions, it is well established that excluded volume effects are the responsible for partitioning. For that reason models for diverse situations and geometries have been devised[4–8] since the pioneering work of Ogston, who derived an expression for the partition coefficient in the case of spherical solute into a solution of randomly arranged fibers.[9] This expression has been widely employed and, recently, it has been applied to calculate the interactions between nanogels.[10]

Some of these models have been extended to macromolecular charged solutes (e.g., proteins, colloidal particles).[11,12]For instance, Johnson and Deen modified Ogston's model by using a Boltzmann factor that contained an electrostatic free energy to modify

the probability of fitting a sphere in a space between fibers.[11] In this approach, however, ions were only accounted for through the Debye screening parameter.

Other authors have been interested in the partitioning of cations and anions rather than highly charged macromolecular species.[13–17] When only small ions are present, excluded volume effects are usually neglected and partitioning is generally explained in terms of an *ideal* Donnan exclusion, i.e., the reduction in concentration of mobile ions within a permeable membrane due to the presence of fixed ions of the same sign as the mobile ions.[13–15,18] In this case, an expression for the Donnan potential difference (ψ_D) between the gel and the reservoir can be obtained from the condition of overall electroneutrality within the gel:

$$\psi_D = \frac{k_B T}{ze} \ln\left(\sqrt{1 + \left(\frac{z_{FG} c_{FG}}{2 z c_{res}} \right)^2} + \frac{z_{FG} c_{FG}}{2 z c_{res}} \right) \qquad (1)$$

Where k_B is Boltzmann's constant, e the elementary charge, T the absolute temperature, z_{FG} the valence of the fixed charged groups of the gel, c_{FG} the concentration of such groups, z the absolute value of the valence of the symmetrical electrolyte, and c_{res} its concentration at the reservoir.

An exception in which excluded volume effects were partially considered for partitioning of conventional electrolyte solutions is the work performed by Fatin-Rouge *et al.*[16] These authors treated the exclusion due to volume, Donnan and specific effects separately, in such a way that the partition coefficient was expressed as a product of steric, electrostatic (Donnan) and specific effects. They employed the pore model for the description of volume exclusion but steric effects were not taken into account in Donnan exclusion. In other words, Fatin-Rouge *et al.* used the expression for the Donnan potential that assumes point ions (Equation 1). Some author have however

found failures of this classical approach for moderately charged hydrogels or in the presence of multivalent ions.[19,20]

Very recently, Dursch*et al.* have also shown that the so-called enhancement factor (defined as the quotient between the partition coefficient and the hydrogel water volume fraction) can also be expressed as a product of the enhancement factors corresponding to steric, electrostatic and specific interactions.[17] Unlike Fatin-Rouge *et al.*, Dursch and coworkers have employed an expression for Donnan exclusion that does account for excluded volume effects. Jha et al. have also proposed a modified Donnan theory for nanogels that considers ion-ion exclusion and even predicts swelling at high salt concentrations.[21]

The theoretical expressions put forward by Fatin-Rouge *et al.*[16] and Dursch*et al.*[17] were applied to the partitioning of common electrolytes and small drug molecules in agarose and 2-hydroxyethyl methacrylate/methacrylic acid hydrogels. These expressions are user-friendly and can be very useful for experimentalists providing that their validity is previously tested. For instance, Fatin-Rouge *et al.* reported specific interactions between metal ions and the gel.[16] Unfortunately, a recent work has shown that the pore model (employed by these authors) provides a poor description of such effects in the case of cross-linked polymer networks.[22] Thus the deviations induced by such a description might be erroneously attributed to other effects and lead to wrong conclusions. For instance, recent simulations have explained why pore sizes obtained from the pore model by fitting experimental partitioning data are systematically overestimated.[22]

Computer simulations are extremely helpful when tailor-made systems are highly recommended. Indeed diverse aspects of partitioning in fibrous media (such the effect of the solute concentration) have been investigated through simulations. In these works, fibers were usually modeled as separate cylinders. In a recent work,[22] however, gels

have been modeled as crosslinked sequences of beads. In this way, certain aspects of real gels such as flexibility and crosslinking were accounted for. In fact, some researchers have also simulated charged gels within diverse bead-spring models of polyelectrolyte,[23–30] in which a single bead represent a small group of atoms (coarse graining).[30,31] This powerful tool, which has been also employed in studies on adsorption and collapse of polyelectrolytes,[32–41] is particularly helpful for the analysis of some non-specific aspects on gels, such as charge and size effects, since electrostatic and excluded-volume interactions can be explicit and directly considered. As an additional illustrative example, we might comment that very recent coarse-grained simulations have studied polyelectrolyte gels as a tool for specific viral detection.[42]

According to the preceding introduction, our main objective is to propose and test a simple model for considering excluded volume effects on ionic partitioning in gels. We will also pay special attention to the effect of size exclusion on Donnan exclusion. It should be mentioned, however, that our work is restricted to the partitioning induced by nonspecific forces. Very recently, a theoretical approach has focused on the role played by specific interactions in ionic partitioning.[43]

MODEL AND SIMULATION.

Model.

The usual model for gels and microgels consists in an idealized representation of a polymer network in which monomer units and cross-linkers are modeled as spheres of diameter d_m. Each polymer chain is considered a sequence of a given number of spherical monomer units (beads), designated by N_{bead}. The number of fixed charged beads per chain and the corresponding fraction are symbolized by $N_{charged}$ and f ($=N_{charged}/N_{bead}$), respectively. The charge of every fixed charged group is $-e$ (i.e.,

$z_{FG} = -1$). Four polymer chains can be connected to every crosslinker molecule. Ions (with their corresponding hydration shells) are also modeled as spheres. As usual in many coarse-grained models, the solvent is only taken into account though its relative permittivity, ε_r. What we actually simulate is a small and inner piece of the gel (or microgel), assuming that the rest of the network, replicated through periodic conditions, behaves in the same manner. In this work, we set d_m=0.7 nm since many monomers used in pharmaceutical applications have diameters close to this value.[22] The short-range repulsion between any pair particles due to excluded volume effects can be modeled by means of purely repulsive Weeks–Chandler–Andersen potential:[25,26,28,44]

$$u_{LJ}(r) = \begin{cases} 4\varepsilon_{LJ}\left(\frac{d^{12}}{r^{12}} - \frac{d^6}{r^6} + \frac{1}{4}\right) & r \le \sqrt[6]{d} \\ 0 & r > \sqrt[6]{d} \end{cases} \qquad (2)$$

where r is the centre-to-centre distance between a given pair of particles, ε_{LJ}=4.11·10^{-21} J and $d = (d_i + d_j)/2$ .All the charged species (charged monomers and ions) interact electrostatically through the Coulomb potential:

$$u_{elec}(r) = \frac{q_i q_j}{4\pi\varepsilon_0\varepsilon_r r} \qquad (3)$$

where q_i is the charge of species i and ε_0 is the permittivity of vacuum. Consecutive beads of a chain are connected by harmonic bonds, whose interaction potential is:[23,24,33,45]

$$u_{bond}(r) = \frac{k_{bond}}{2}(r - r_0)^2 \qquad (4)$$

where k_{bond} is the elastic constant (k_{bond}=0.4 N/m) and r_0 is the equilibrium bond length.

Simulations.

As mentioned previously, gels have the ability to change their volume in response to environmental stimuli. In this work, however, the mechanisms responsible for the

swelling or collapse of gels do not concern us. For that reason, the different volume fractions in which we are interested are simulated just adjusting the dimensions of the simulation cell while the number of particles of the network remains fixed. In other words, the network is simulated in the canonical ensemble, in which volume, temperature and the number of particles of the network remain fixed. Periodic boundary conditions were applied to the cubic simulation box that contained the particles of different species, including 8 nodes and 16 polymer chains. Different authors have employed these numbers of nodes and polymer chains in similar simulations.[23–26,44–46] Some of them have additionally checked that the effect of the cell size is not important for the computation of certain global properties (such as the gel volume, or the osmotic pressure) comparing with results for 8-fold larger cells.[23,44] In this work, we have also checked that cell size hardly affects the computation of partition coefficients employing these cells. In any case, the nodes were initially positioned on a diamond lattice whereas the monomer beads were distributed along the lines connecting them. Boltzmann-weighted configurations were generated using the conventional Metropolis Monte Carlo (MC) protocol.

It should be mentioned, however, that the electrolyte in equilibrium with the reservoir was simulated in the grand canonical ensemble implementing the method of Valleau and Cohen.[47] The MC simulation in the GC ensemble consists of three moves (displacement, insertion and removal). As the condition of electrical neutrality of a system had to be preserved, electroneutral groups of p cations and q anions were inserted at random positions or were randomly selected from the ions contained in the box and removed when insertions or removals were attempted, respectively. The probability of acceptance of these trial moves were given by:

$$acc(insertion) = \min\left[1, \exp\left(-\frac{\Delta u_c}{k_B T} + \ln\frac{(c_{res} N_A V\gamma)^p}{\prod_i^p (N_+ + i)} + \ln\frac{(c_{res} N_A V\gamma)^q}{\prod_i^q (N_- + i)}\right)\right] \quad (5)$$

$$acc(removal) = \min\left[1, \exp\left(-\frac{\Delta u_d}{k_B T} + p\ln\frac{N_+}{c_{res} N_A V\gamma} + q\ln\frac{N_-}{c_{res} N_A V\gamma}\right)\right] \quad (6)$$

Where: N_A is Avogadro's number, V is the volume of the simulation cell, Δu_c and Δu_d are the potentials of creation and destruction, respectively, N_+ and N_- are the current numbers of ions before the insertion or removal attempts, and γ is the mean activity coefficient, which must be determined from a pure electrolyte simulation before simulating the gel.

THEORY

Expressions for the Donnan potential difference and partition coefficients.

In this section, an approximate analytical expression for the partition coefficient will be derived. Phase equilibrium requires that solute chemical potential in the reservoir equals the chemical potential inside the gel:

$$\mu_i^0 + z_i e\psi^{res} + k_B T \ln c_i^{res} = \mu_i^0 + z_i e\psi^{gel} + k_B T \ln c_i^{gel} + \mu_i^{exc} \quad (7)$$

Where μ_i^0 is the ideal solution standard-state chemical potential (per particle) for uncharged point ions of species i, z_i is the valence of species i, ψ^{res} and ψ^{gel} are the electrostatic potential at the reservoir and the gel, respectively, c_i^{res} and c_i^{gel} are the concentrations of species i at the reservoir and the gel, respectively, and μ_i^{exc} is the excess chemical potential (of species i) associated to excluded volume effects in the gel. Two ionic species are considered in this work: monovalent cations (i=1, counterions in our case, $z_1 = +1$) and monovalent anions (i=2, coions, $z_2 = -1$). The reader should keep in mind that: i) c_2^{gel} equals the concentration of electrolyte inside the gel coming

from the reservoir; ii) $c_1^{gel} > c_2^{gel}$ for $f > 0$ (charged network), since c_1^{gel} not only includes the counterions coming from the external electrolyte but also those neutralizing the fixed charged groups of the gel. In addition, the condition of electroneutrality demands:

$$z_1 c_1^{gel} + z_2 c_2^{gel} + z_{FG} c_{FG} = 0 \tag{8}$$

From Equation 7, it can be easily shown that:

$$K_i \equiv \frac{c_i^{gel}}{c_i^{res}} = \exp\left(\frac{-\mu_i^{exc}}{k_B T}\right)\exp\left(\frac{-z_i e\psi_D}{k_B T}\right) \tag{9}$$

where $\psi_D = \psi^{gel} - \psi^{res}$ and K_i is the partition coefficient. Dividing each term of Equation 8 by $c_1^{res} = c_2^{res} = c^{res}$, setting $z_1 = +1$ and $z_2 = -1$, inserting Equation 9 (with *i*=1 and 2), and solving for ψ_D yields:

$$\psi_D = -\frac{k_B T}{e}\ln\left(\sqrt{\frac{\exp\left(-\frac{\mu_2^{exc}}{k_B T}\right)}{\exp\left(-\frac{\mu_1^{exc}}{k_B T}\right)} + \left(\frac{z_{FG} c_{FG}}{2c^{res}\exp\left(-\frac{\mu_1^{exc}}{k_B T}\right)}\right)^2} - \frac{z_{FG} c_{FG}}{2c^{res}\exp\left(-\frac{\mu_1^{exc}}{k_B T}\right)}\right) \tag{10}$$

It can be easily shown that Equation 10 reduces to Equation 1 when excluded volume effects are neglected ($\mu_i^{exc} = 0$). In any other case, however, the Donnan potential difference depends on finite size effects. In other words, excluded volume and electrostatic effects are coupled in partitioning since, according to Equations 9 and 10, the partition coefficient cannot be expressed as the product of two completely independent factors associated to the corresponding effects. At this point, it is worth mentioning that c_{FG} can be estimated from the polymer volume fraction as:

$$c_{FG} \approx \frac{6\varphi_p f}{\pi d_m^3} \tag{11}$$

Approximate expressions for the excluded volume chemical potential.

In any case, μ_i^{exc} must be specified to predict partition coefficients. In general, chemical potentials depend on ionic concentrations inside the gel, c_i^{gel}. Thus, after inserting Equation 10 and specifying μ_i^{exc}, Equation 9 involves a set of two algebraic equations (whose unknown quantities are c_1^{gel} and c_2^{gel}) that must be solved numerically if approximations are not used. In this work, however, we will provide an approximate analytical expression for the partition coefficient that depends on the polymer volume fraction but does not depend on c_i^{gel}, which considerably facilitates its application in practice.

If the polymer and ionic volume fractions are low enough, μ_i^{exc} can be expressed as:[8,48]

$$\frac{\mu_i^{exc}}{k_B T} = \alpha_{i1}\varphi_1 + \alpha_{i2}\varphi_2 + \alpha_{ip}\varphi_p \qquad (12)$$

where φ_1 and φ_2 are the volume fractions of ions 1 and 2 (counterions and coions), respectively, and α_{ij} (with j=1, 2 and p, ions 1, 2 and polymer) are geometrical factors whose functional form is:[7]

$$\alpha_{ij} = \left(1 + \frac{d_i}{d_j}\right)^n \qquad (13)$$

Where, d_i is the diameter of species i, n=3 for two spherical species and n=2 when the exclusion between a sphere and a cylinder is considered (recovering Ogston's formula in this case). Obviously, n=3 for α_{i1} and α_{i2} since ions are modeled as spheres, but the n-value for α_{ip} deserves some discussion. As the polymer chain is modeled a sequence of spherical beads, one might initially think that n=3 as well. However, a previous work has shown that this necklace can be modeled as a fiber (cylinder) of diameter d_m if the solute is large enough. In this case, n=2.[22]

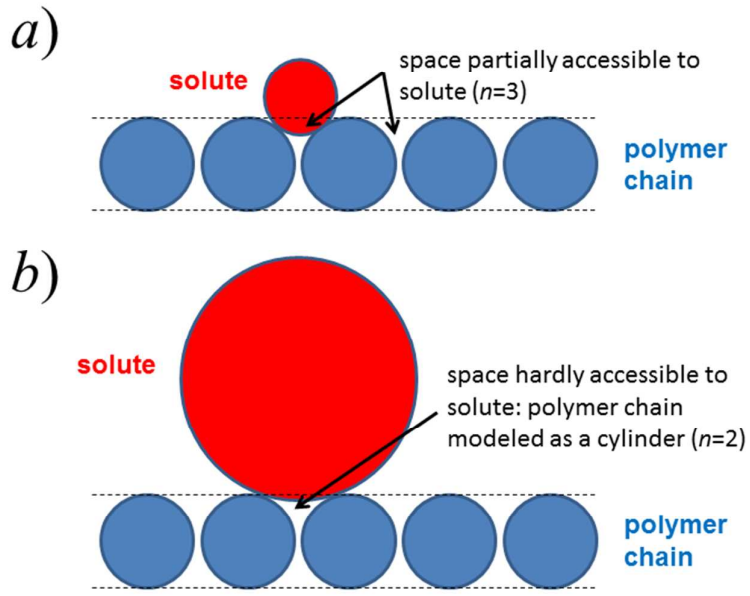

FIGURE 1. Schematic picture illustrating the meaning of exponent *n*. a) Solutes with sizes comparable to or smaller than the monomer units can partially access to the space between them (*n*=3); b) Large solutes (compared to monomer units) can hardly access to the space between them and, consequently, the polymer chain can be modeled as a cylinder (*n*=2).

Figure 1 can help us to understand the reason for this. As can be seen, solute particles can partially occupy the space between adjacent polymer beads if the dimensions of the solute molecules are comparable to or smaller than the monomer dimensions. In this case, the polymer chain can be really modeled as a sequence of beads and *n*=3. However, the situation becomes different when the solute is much greater than the polymer beads since the interstices between adjacent beads are not accessible. In this case, the polymer chain can be thought of as a fiber (*n*=3) rather than a sequence of spheres. In this work, these two limit values will be considered for *n* (2 and 3).

As we have previously supposed, Equation 12 involves c_1^{gel} and c_2^{gel} through φ_1 and φ_2, respectively, which are just the quantities that we want to predict. In order to avoid

advanced numerical treatments, we will also assume that φ_2 is negligible as compared to φ_p. This assumption seems sound if the electrolyte concentration at the reservoir is low enough and/or the gel is moderately (or highly) collapsed and, in any case, it implies that c_2^{gel} is negligible as well. In turn, this means that $c_1^{gel} \approx c_{FG}$. Accordingly, φ_1 can be estimated from φ_p, as follows:

$$\varphi_1 \approx \frac{\pi}{6} c_{FG} d_1^3 = \frac{\pi}{6} \frac{6\varphi_p f}{\pi} = \frac{d_1^3}{d_m^3} f\varphi_p \qquad (14)$$

Thus we finally obtain:

$$\frac{\mu_i^{exc}}{kT} \approx \left[\left(1 + \frac{d_i}{d_1}\right)^3 \frac{d_1^3}{d_m^3} f + \left(1 + \frac{d_i}{d_m}\right)^n \right] \varphi_p \qquad (15)$$

Inserting this approximate result into Equations 10 and 9 leads to easy and straightforward predictions of the Donnan potential difference and the partition coefficient providing that φ_p is known. The reader should bear in mind that Equation 15 accounts for not only volume exclusion associated to the polymer but also finite size effects associated to the counterions that neutralize the charge of the network, whose contribution is also proportional to φ_p. This constitutes a novelty itself.

As mentioned previously, after specifying μ_i^{exc}, Equations (9) and (10) constitute a set of coupled algebraic equations, which can be numerically solved. To figure out if the approximations that lead to analytical expressions ($\varphi_2 \approx 0$ and Equation 14) are reasonable, the predictions obtained for K_2 from such analytical expressions were compared to the numerical solution of this set of equations. For 0.7/0.7 electrolytes, the results were almost identical. For 2.8/0.7 electrolytes, some small differences were found. Just as an example, Figure 2 shows the numerical and approximate solutions for 2.8/0.7, n=2 and f ranging from 0.0208 to 0.50. As can be seen, the K_2-values obtained numerically are slightly smaller than the approximate ones, but the discrepancies can be

observed only at low polymer volume fractions and low *f*-values. This is logical since, in this case, φ_2 is *not* negligible as compared to φ_p or φ_1 (approximation involved).

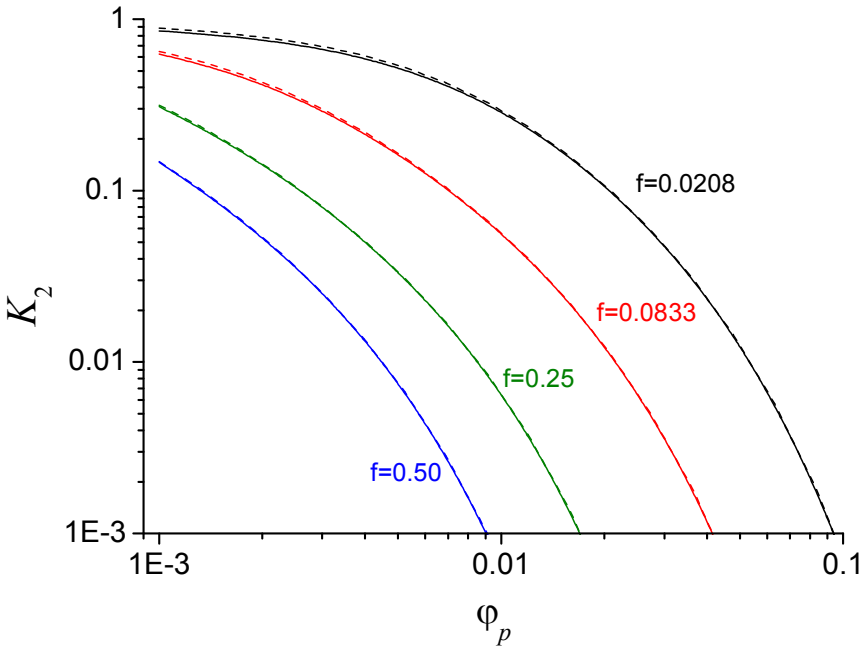

FIGURE 2. Partition coefficient K_2 obtained from theoretical predictions as a function of the polymer volume fraction for networks with different *f*-values (f = 0.0208, 0.0833, 0.25 and 0.50) in the presence of the electrolyte 2.8/0.7. Theoretical predictions were obtained from the numerical solution of the set of coupled equations (9, 10 and 12) (solid lines) and using the approximation given by equation 15 (dashed lines).

RESULTS

In this work, we have simulated gels with polymer chains of 48 beads (N_{bead}= 48) at 298 K. In the main set of simulations, a reservoir electrolyte concentration of 1 mM was chosen. Four monovalent electrolytes with different ionic sizes, summarized in Table 1, have been studied in this work.

As can be seen, all the electrolytes that appears in this table include at least one type of ion (cation and/or anion) with d_i = 0.7 nm. This ionic size is representative for many hydrated monatomic cations and anions (if the hydration shell is included)[49] as well as some drugs (e.g., theophylline, caffeine).[17] However, other drugs with ionized groups

have greater diameters (e.g., hydrocortisone, acetazolamide).[17] Thus it would be interesting to explore what happen if one of the ions has a greater size. For this reason, ions with deliberately larger diameters (d_i = 2.8 or 3.5 nm) have been also included in our survey.

TABLE 1. Ionic sizes and mean activity coefficients (at 1 mM) of the electrolytes analyzed here.

Electrolyte	Counterion diameter (d_1), nm	Coion diameter (d_2), nm	Mean activity coefficient (γ)
0.7/0.7	0.7	0.7	0.9706
2.8/0.7	2.8	0.7	1.0115
3.5/0.7	3.5	0.7	1.0551
0.7/2.8	0.7	2.8	1.0116

For the ionic sizes explored in this survey, this implies ionic volume fractions that range from 0.0001 to 0.01 (in round numbers). Consequently, such a reservoir concentration can be considered dilute for many purposes (such as some previous assumptions made in the theoretical model). First, it is quite instructive to analyze the predictions of Donnan potential difference obtained from Equations 10 and 15 for the different electrolytes mentioned previously and a slightly charged gel (f = 0.0208, more charged networks will be discussed later).

Figure 3 shows such predictions for the four above mentioned electrolytes. n=2 was applied. The prediction in the absence of finite size effects is also plotted for comparison. As can be seen, the deviations of ψ_D from the ideal behavior for counterions of 0.7 nm are not significant for polymer volume fractions below 0.1. In contrast, the deviations from the ideal behavior caused by excluded volume effect significantly increase when the counterion diameter grows.

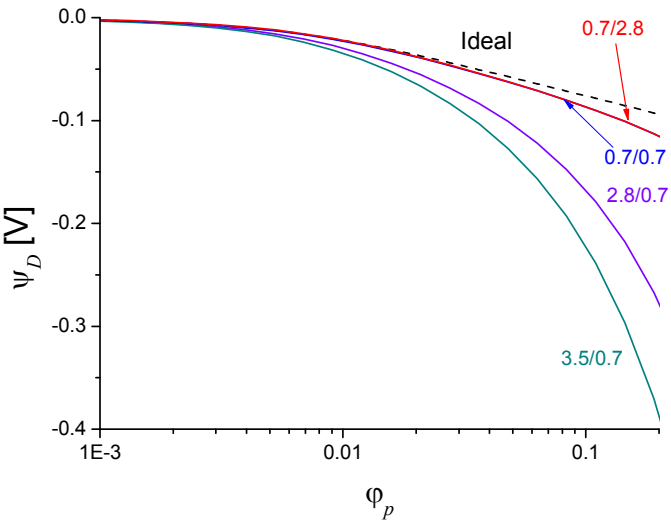

FIGURE 3. Donnan potential difference predicted by Equations 10 and 15 as a function of the polymer volume fractions for a network with f = 0.0208 and n=2 in the presence of four different electrolytes: 0.7/0.7, 0.7/2.8, 2.8/0.7 and 3.5/0.7. The prediction of Equation 1 (ideal Donnan) is also plotted (dashed line).

Now it is interesting to look into how partitioning deviates from the ideal Donnan exclusion partitioning when finite size effects are accounted for. Figure 4 shows the partition coefficient obtained from simulation as a function of the polymer volume fraction for the same system and conditions as in Figure 3. The prediction assuming ideal Donnan exclusion is also plotted for comparison. Given that c_2^{gel} tells us the concentration of electrolyte coming from the reservoir, we have preferred to analyze K_2.

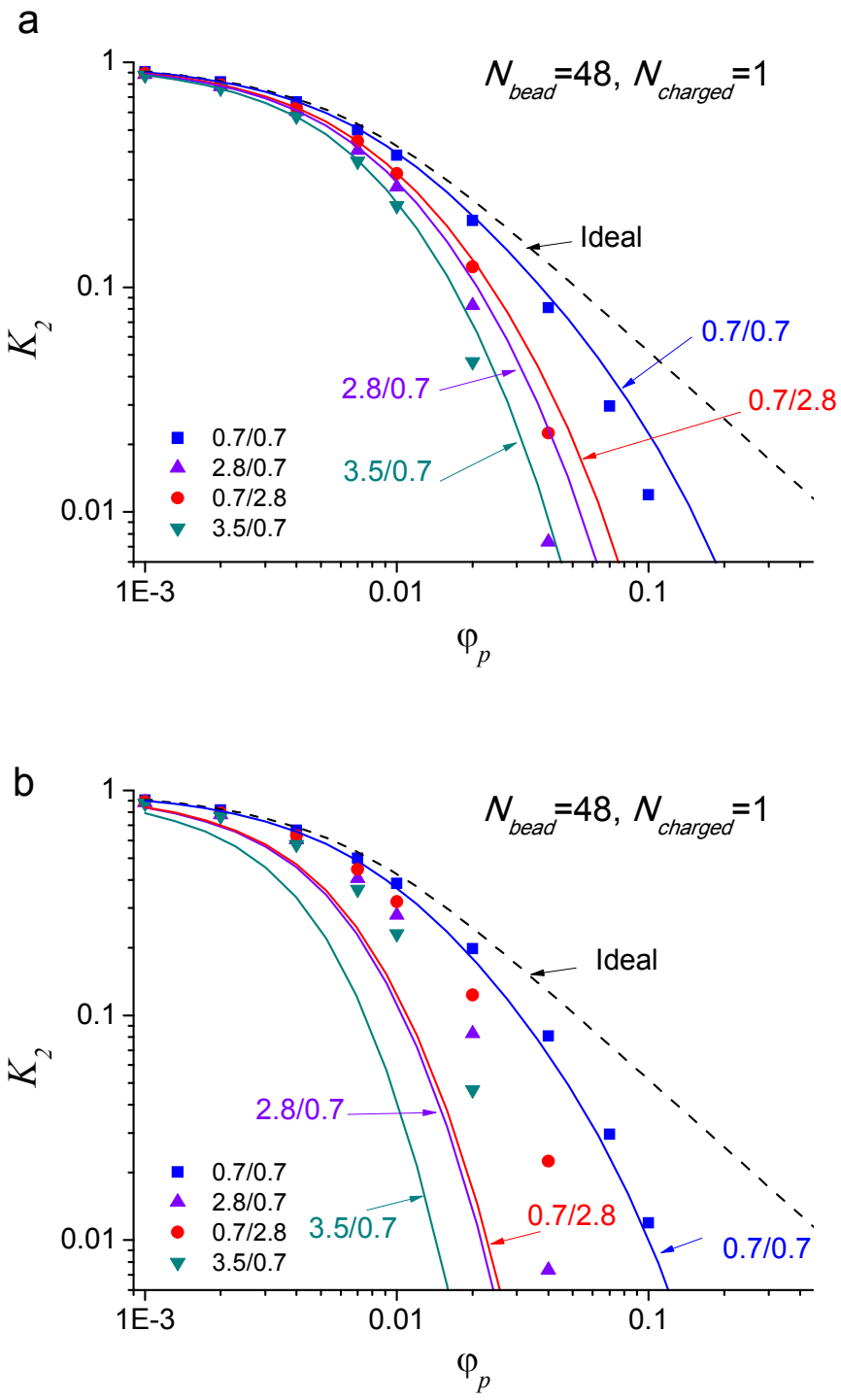

FIGURE 4. Partition coefficient K_2 obtained from simulations as a function of the polymer volume fractions for a network with $f = 0.0208$ in the presence of four different electrolytes: 0.7/0.7 (squares), 0.7/2.8 (circles), 2.8/0.7 (up triangles) and 3.5/0.7 (down triangles). Theoretical predictions obtained from Equations 9, 10 and 15 (solid lines) for n=2 and n=3 are also plotted in Figures 4a and 4b, respectively. The prediction ideal Donnan exclusion is also plotted (dashed line).

In relation to this figure, it should be first stressed the importance of ionic size in partitioning. Figure 4 clearly reveals that the partition coefficient draws away from the ideal Donnan exclusion when the size of counter- or coions grows. More specifically, the discrepancies increase following the sequence: 0.7/0.7, 0.7/2.8, 2.8/0.7 and 3.5/0.7. The predictions obtained after inserting ψ_D into Equation 9 are also plotted for n=2 (polymer chain modeled as cylinder or fiber) and n=3 (polymer chain modeled as sequence of beads) in Figure 4a and 4b, respectively. As can be seen in Figure 4a, the agreement between theory and simulation is good (taking the simplicity of the model into account) not only qualitatively but also quantitatively for n=2. For n=3 (Figure 4b) the agreement between theory and simulation is slightly better for the electrolyte 0.7/0.7, which suggests that polymer chains behave as sequences of beads rather than fibers. However, the predictions obtained with n = 2 for 0.7/2.8, 2.8/0.7 and 3.5/0.7 are clearly better than those obtained with n = 3. This means that, theoretically speaking, polymer chains can be modeled as fibers when greater ions are present. As mentioned above, the interstices between adjacent beads of the polymer chains are hardly accessible for large solute particles. This also explains why such chains are seen as cylinders rather than a sequence of spheres.

At this point, it is interesting to analyze the effect of charge. In the following subset of simulations, different fractions of charged monomers were simulated for the 0.7/0.7 electrolyte: f = 0.0208, 0.0833, 0.25and 0.50 (corresponding to $N_{charged}$ = 1, 4, 12 and 24, respectively). Figure 5 shows the corresponding partition coefficients as a function of the polymer volume fraction. The predictions obtained from Equations 10, 11 and 12, with n = 2 are also plotted. As can be seen, the agreement between theory and simulation is good for slightly charged gels (f = 0.0208 and 0.0833). When f is increased up to 0.25, some numerical discrepancies appear between theory and simulations. This

disagreement clearly grows for f = 0.50. As can be seen, the K_2-values obtained from simulations are greater than those predicted by Equation 12.

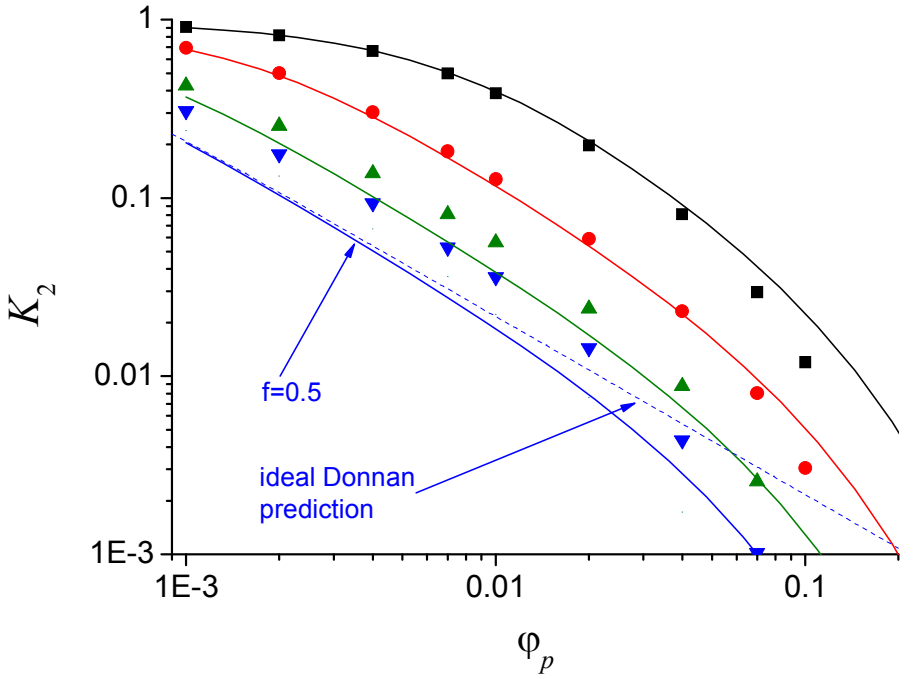

FIGURE 5. Partition coefficient K_2 obtained from simulations as a function of the polymer volume fractions for networks with f = 0.0208 (squares), 0.0833 (circles), 0.25 (up triangles) and 0.50 (down triangles) in the presence of the electrolyte 0.7/0.7. Theoretical predictions with n=2 (solid line) are also plotted. In the case of f=0.5, the prediction obtained from the assumption of ideal Donnan exclusion was also included.

This happens even for low volume fractions, when excluded volume effects are negligible and the prediction that includes such effects tends to the ideal Donnan exclusion. These differences cannot be attributed to the approximations made to obtain analytical expressions for the partition coefficient, since the numerical solution is even slightly smaller than the analytical one (as seen in Figure 2). Thus the failure of the theory for moderately charged gels could be attributed to electrostatic (Donnan) effects. Recently, Höpfner *et al*. have also reported that the classical Donnan approach underestimates the concentration of salt inside the gel for moderately charged hydrogels. These authors employed a similar model but their work is restricted good

solvent conditions (when excluded volume effects are not expected to play an important role) and smaller ions (d_i=0.35 nm).

To understand why the assumption of ideal Donnan exclusion does not work at 1 mM if f is high, it is worth analyzing the counterion-counterion radial distribution function (rdf), $g_{11}(r)$. Figure 6 shows this function for 0.0833 and 0.50, two f-values corresponding to low and highly charged networks. As can be seen, $g_{11}(r)$ vanishes for distances smaller that contact distance (0.7 nm) as a result of the short-range repulsion between any pair of particles.

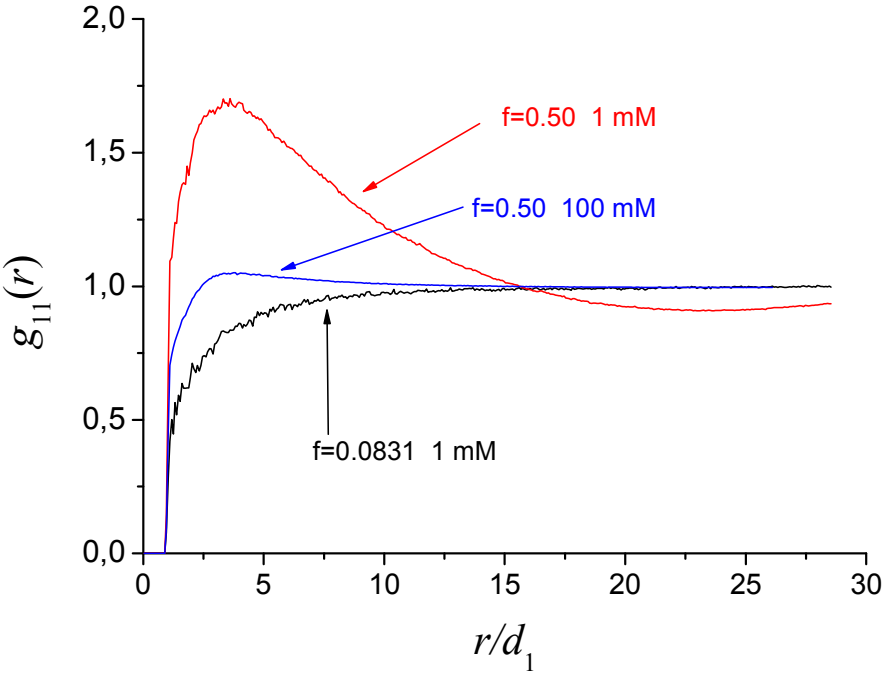

FIGURE 6. Counterion-counterion radial distribution function, $g_{11}(r)$, for three networks in the presence of 0.7/0.7 electrolyte: f = 0.0831 and 1 mM; f = 0.5 and 1 mM; f = 0.5 and 100 mM.

For larger distances, this radial distribution function (rdf) is very close to 1, which means that the effective electrostatic repulsion between counterions is negligible and these particles behave as an ideal gas. However, when f increases up to 0.50 the

situation noticeably changes, since the rdf exhibits a high peak. Thus these particles are now spatially ordered and the hypothesis of ideal gas does not hold anymore. As Equation 1 was derived under this assumption, it is not surprising that the ideal Donnan exclusion fails to predict the partition coefficient even at low polymer volume fractions. Finally, Figure 6 also shows the rdf for f=0.5 and 100 mM. As can be seen, the peak that the gel with f=0.5 exhibits at 1 mM has disappear as a result of the electrostatic screening at high ionic strength. Thus the classical Donnan approach should work better under such conditions. This will be confirmed later.

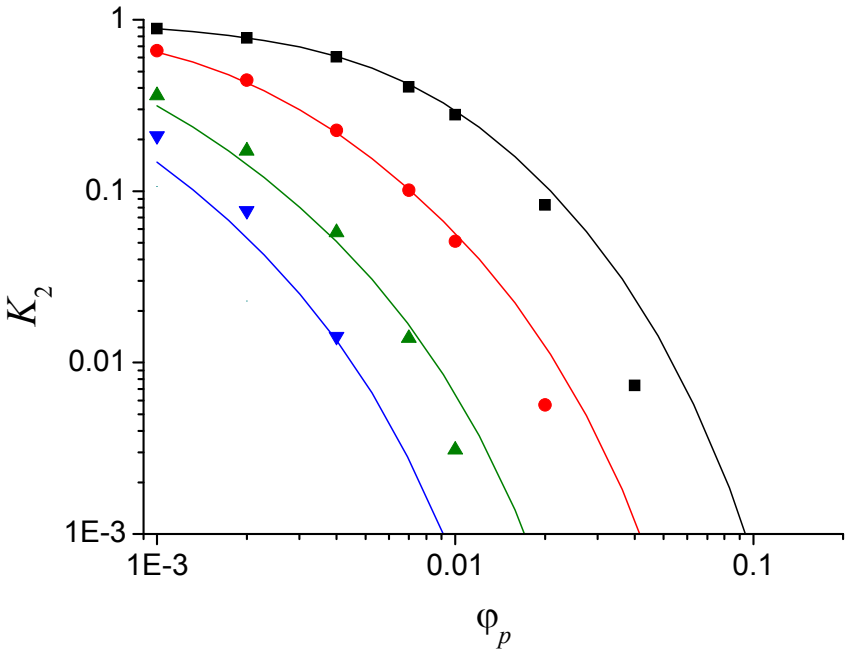

FIGURE 7. Partition coefficient K_2 obtained from simulations as a function of the polymer volume fractions for networks with different f-values in the presence of the electrolyte 2.8/0.7. Same legend as Figure 5.

After analyzing the effect of charge on the partitioning of the electrolyte solute with identical ionic sizes (0.7/0.7), we turn our attention to electrolytes with counterions greater than coions. Figures 7 and 8 show the partition coefficients provided by

simulations for the same set of *f*-values, but with electrolytes 2.8/0.7 and 3.5/0.7, respectively. Theoretical predictions for $n = 2$ are also plotted.

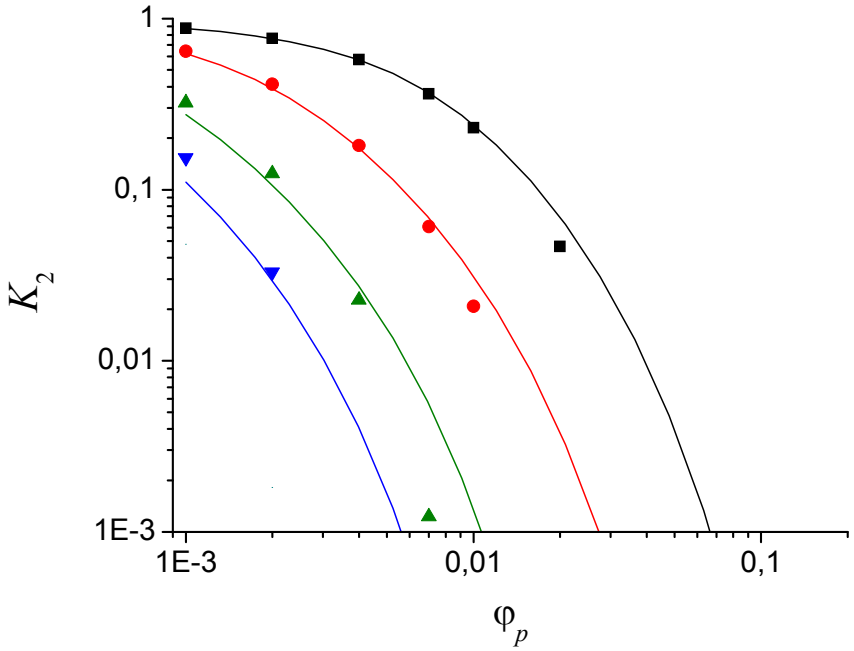

FIGURE 8. Partition coefficient K_2 obtained from simulations as a function of the polymer volume fractions for networks with different *f*-values in the presence of the electrolyte 3.5/0.7. Same legend as Figure 5.

It should be mentioned that some quantitative agreement between simulation and theoretical predictions is now found for f=0.5, in contrast with the discrepancies reported for 0.7/0.7, previously discussed (see Figure 5). This somewhat surprising agreement could be justified as follows. First, the partition coefficient predicted by the ideal Donnan exclusion, which governs the behavior at low volume fractions, does not change when the counterions of 0.7 nm are replaced by counterions of 2.8 nm. However, the K_2-values obtained from simulations reduce because accommodating large ions is more difficult. As a result of these effects, simulation and predictions of

ideal Donnan exclusion tends to approach at low polymer volume fractions. The agreement at higher φ_p-values is achieved accounting for excluded volume effects.

Regarding partitioning of electrolytes at low concentration (1 mM in this work), we finally analyze what happens if electrolytes with large coions (instead of conterions) are considered. Figure 9 shows the partition coefficients for the same set of *f*-values but now for the electrolyte with coions of 2.8 nm (0.7/2.8). In this case, the behavior resembles that reported for counterions of 0.7 nm. For $f = 0.5$, theoretical predictions again underestimate the partition coefficient, as reported for these counterions. The reasons argued in that case could be valid now.

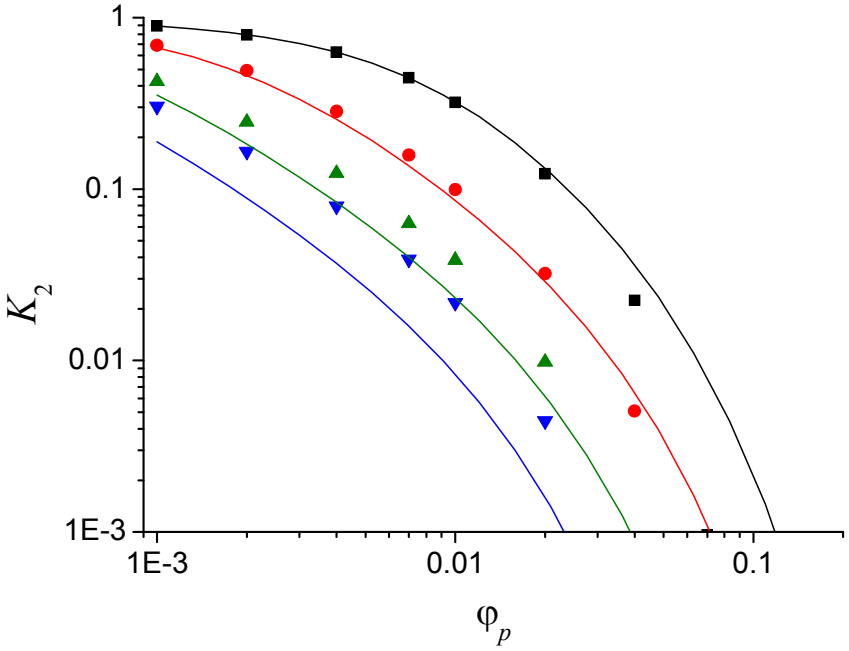

FIGURE 9. Partition coefficient K_2 obtained from simulations as a function of the polymer volume fractions for networks with different *f*-values in the presence of the electrolyte 0.7/2.8. Same legend as Figure 5.

We might then wonder why the accidental agreement between theory and simulation reported for counterions of 2.8 and 3.5 nm and networks with f=0.5 is not observed in

this case. To answer this question we should recall that, for high *f*-values and 1 mM, counterions are much more numerous than coions.

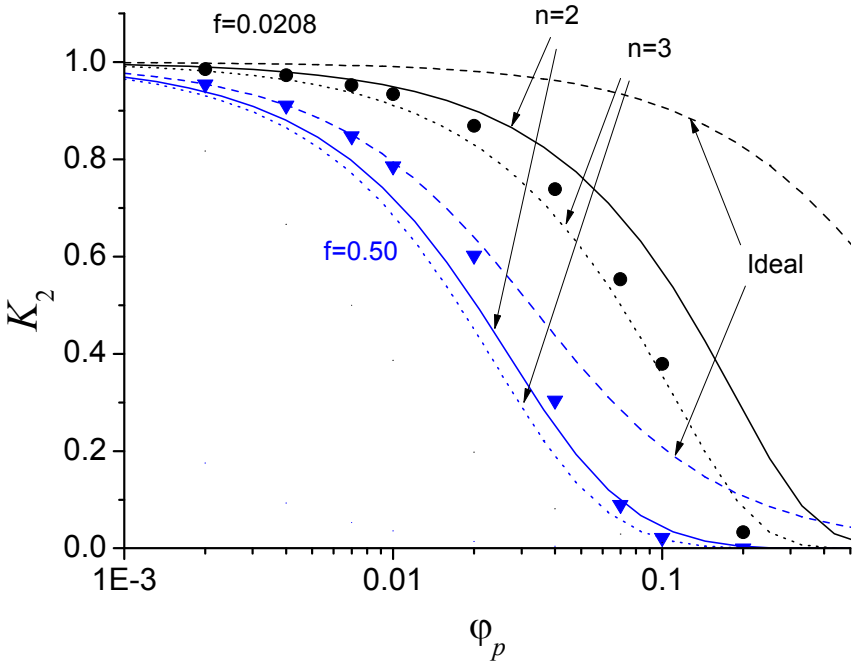

FIGURE 10. Partition coefficient K_2 obtained from simulations as a function of the polymer volume fractions for networks with f=0.0208, (circles) and 0.50 (down triangles) in the presence of the electrolyte 0.7/0.7 at 100 mM. Theoretical predictions with n=2 (solid line) and n=3 (dotted line) are also plotted. The predictions obtained from the assumption of ideal Donnan exclusion were also included (dashed line).

Thus accommodating external counterion/coion pairs in the network is more difficult only if the excess counterions neutralizing the gel are greater. In other words, 0.7/0.7 and 0.7/2.8 ionic pairs can enter the gel with similar difficulty. In fact, the reader can check that the partition coefficients (obtained from simulation) at low volume fraction (say φ_p=0.001) for electrolytes 0.7/0.7 and 0.7/2.8 are almost identical (≈0.3).

Although this work has been focused on the partitioning of relatively dilute electrolytes (1 mM), we would like to show a few results for more concentrated solutions. Figure 10 shows the partition coefficient of a 0.7/0.7 electrolyte at 100 mM as a function of φ_p for

gels with f = 0.0208 and 0.50. The predictions obtained from n = 2, 3, and the ideal Donnan exclusion are also plotted. To begin with, let us analyze the results for the slightly charged gel. First, it should be stressed that the partition coefficient predicted by the ideal Donnan exclusion decays much more slowly than that obtained from simulations. This obviously suggests that the role played by excluded volume effects in partitioning is now much more important. In relation to this, the reader should recall that we are dealing with the 0.7/0.7 electrolyte. If greater ions were considered, the discrepancies between ideal Donnan exclusion and simulations would be even larger. When excluded volume effects are taken into account, theoretical predictions are much better. More specifically, the best agreement is achieved for n = 3, which means that the interstices between adjacent monomer beads are partly occupied by ions.

When f increases up to 0.50, the role played by Donnan exclusion is expected to be more important. This agrees with Equation 1, which predicts greater Donnan potential values (in magnitude) for larger concentrations of charged groups (c_{FG}). In fact, the assumption of ideal Donnan exclusion works reasonably well at low polymer volume fractions, which contrasts with the disagreement found in Figure 5 (for the same f-value, 0.50). In relation to this, we should keep in mind that electrostatic interactions (responsible for the spatial ordering observed in Figure 6) are much more screened at 100 mM than at 1 mM. This was corroborated in Figure 4, where the rdf for f = 0.50 and 100 mM was also included. As mentioned before, the peak of this function at 100 mM is much smaller than at 1 mM. Consequently, counterions are less ordered at 100 mM and their behavior is more ideal. At any case, Figure 10 also reveals that the theoretical predictions accounting for excluded volume effects work better than those derived from Equation 1 at intermediate and high polymer volume fractions.

CONCLUSIONS.

Our CG simulations reveal that excluded volume effects on ionic partitioning in swollen and moderately collapsed gels can be important and produce deviations from the classical theory of Donnan exclusion at low or moderate reservoir electrolyte concentration if one of the ions has diameters of just a few nanometers (e.g., some drugs with ionized groups). For larger reservoir electrolyte concentrations, volume exclusion can become the dominant effect and lead to the severe failure of the ideal Donnan exclusion even for subnanometer ions, such as conventional hydrated monatomic cations. Apart from that, simulations also confirm that the classical theory does not work properly for highly charged gels at low ionic strengths due to the high spatial ordering of counterions.

Additionally, these simulations have allowed us to test an approximate analytical expression for the partition coefficient of ionic species that accounts for the volume exclusion associated to the polymer network and the counterions that neutralize its charge. This theory also provides an expression for the Donnan potential difference that takes such effects into account. Our result shows that reliable predictions of partitioning are obtained for slightly and moderately charged gels (both at low and high reservoir electrolyte concentrations). In these cases, the predictions in which the polymer is modeled as a fiber agree better with simulations for electrolytes with large ions. The theory also works acceptably for highly charged gels at high salt concentrations or for electrolytes with large counterions.

ACKNOWLEDGEMENTS.

The authors thank the financial support from the following institutions: i) ‘Ministerio de Economía y Competitividad, Plan Nacional de Investigación, Desarrollo e

InnovaciónTecnológica (I+D+i)', Projects MAT2012-36270-C04-04 and -02. ii) 'Consejería de Innovación, Ciencia y Empresa de la Junta de Andalucía', Project P09-FQM-4698. iii) European Regional Development Fund (ERDF).

REFERENCES

1. R. Pelton, *Adv. Colloid Interface Sci.*, 2000, **85**, 1–33.
2. J. Ramos, A. Imaz, J. Callejas-Fernandez, L. Barbosa-Barros, J. Estelrich, M. Quesada-Perez, and J. Forcada, *Soft Matter*, 2011, **7**, 5067–5082.
3. N. a Peppas, P. Bures, W. Leobandung, and H. Ichikawa, *Eur. J. Pharm. Biopharm.*, 2000, **50**, 27–46.
4. J. E. Schnitzer, *Biophys. J.*, 1988, **54**, 1065–76.
5. L. A. Fanti and E. D. Glandt, *J. Colloid Interface Sci.*, 1990, **135**, 385–395.
6. L. A. Fanti and E. D. Glandt, *J. Colloid Interface Sci.*, 1990, **135**, 396–404.
7. M. J. Lazzara, D. Blankschtein, and W. M. Deen, *J. Colloid Interface Sci.*, 2000, **226**, 112–122.
8. M. J. Lazzara and W. M. Deen, *J. Colloid Interface Sci.*, 2004, **272**, 288–97.
9. A. G. Ogston, *Trans. Faraday Soc.*, 1958, **54**, 1754–1757.
10. A. Moncho-Jordá, J. A. Anta, and J. Callejas-Fernández, *J. Chem. Phys.*, 2013, **138**, 134902.
11. E. M. Johnson and W. M. Deen, *J. Colloid Interface Sci.*, 1996, **178**, 749–756.
12. M. S. Chun and C. Baig, *Korean J. Chem. Eng.*, 2001, **18**, 816–823.
13. L. P. Yezek and H. P. van Leeuwen, *J. Colloid Interface Sci.*, 2004, **278**, 243–250.
14. L. P. Yezek and H. P. van Leeuwen, *Langmuir*, 2005, **21**, 10342–10347.
15. T. Lopez-Leon, J. L. Ortega-Vinuesa, D. Bastos-Gonzalez, and A. Elaissari, *J. Phys. Chem. B*, 2006, **110**, 4629–4636.
16. N. Fatin-Rouge, A. Milon, J. Buffle, R. R. Goulet, and A. Tessier, *J. Phys. Chem. B*, 2003, **107**, 12126–12137.
17. T. J. Dursch, N. O. Taylor, D. E. Liu, R. Y. Wu, J. M. Prausnitz, and C. J. Radke, *Biomaterials*, 2014, **35**, 620–629.
18. H. Ohshima and T. Kondo, *Biophys. Chem.*, 1990, **38**, 117–122.
19. J. Höpfner, T. Richter, P. Košovan, C. Holm, and M. Wilhelm, in *Intelligent Hydrogels*, eds. G. Sadowski and W. Richtering, Springer International Publishing, 2013, vol. 140, pp. 247–263.

20. C. E. Sing, J. W. Zwanikken, and M. Olvera de la Cruz, *Macromolecules*, 2013, **46**, 5053–5065.

21. P. K. Jha, J. W. Zwanikken, and M. Olvera de la Cruz, *Soft Matter*, 2012, **8**, 9519–9522.

22. M. Quesada-Pérez, I. Adroher-Benítez, and J. A. Maroto-Centeno, *J. Chem. Phys.*, 2014, **140**, 204910.

23. S. Schneider and P. Linse, *J. Phys. Chem. B*, 2003, **107**, 8030–8040.

24. S. Edgecombe, S. Schneider, and P. Linse, *Macromolecules*, 2004, **37**, 10089–10100.

25. B. A. Mann, R. Everaers, C. Holm, and K. Kremer, *Europhys. Lett.*, 2004, **67**, 786–792.

26. B. A. Mann, C. Holm, and K. Kremer, *J. Chem. Phys.*, 2005, **122**, 154903.

27. A. V Dobrynin, *Curr. Opin. Colloid Interface Sci.*, 2008, **13**, 376–388.

28. D.-W. Yin, M. O. de la Cruz, and J. J. de Pablo, *J. Chem. Phys.*, 2009, **131**, 194907.

29. B. A. F. Mann, K. Kremer, O. Lenz, and C. Holm, *Macromol. Theory Simulations*, 2011, **20**, 721–734.

30. P. Košovan, T. Richter, and C. Holm, in *Intelligent Hydrogels*, eds. G. Sadowski and W. Richtering, Springer International Publishing, 2013, vol. 140, pp. 205–221.

31. K. Kremer, *Macromol. Chem. Phys.*, 2003, **204**, 257–264.

32. A. F. Jorge, J. M. G. Sarraguca, R. S. Dias, and A. Pais, *Phys. Chem. Chem. Phys.*, 2009, **11**, 10890–10898.

33. R. S. Dias and A. Pais, *Adv. Colloid Interface Sci.*, 2010, **158**, 48–62.

34. S. Ulrich, M. Seijo, and S. Stoll, *Curr. Opin. Colloid Interface Sci.*, 2006, **11**, 268–272.

35. M. Seijo, M. Pohl, S. Ulrich, and S. Stoll, *J. Chem. Phys.* 2009, **131**, 174704.

36. P. Kosovan, J. Kuldova, Z. Limpouchova, K. Prochazka, E. B. Zhulina, and O. V Borisov, *Soft Matter*, 2010, **6**, 1872–1874.

37. J. M. G. Sarraguca and A. A. C. C. Pais, *Phys. Chem. Chem. Phys.*, 2006, **8**, 4233–4241.

38. M. Seijo, S. Ulrich, M. Filella, J. Buffle, and S. Stoll, *Phys. Chem. Chem. Phys.*, 2006, **8**, 5679–5688.

39. *CRC handbook of chemistry and physics*, CRC Press, 1988.

40. S. J. de Carvalho, R. Metzler, and A. G. Cherstvy, *Phys. Chem. Chem. Phys.*, 2014, **16**, 15539–15550.

41. S. Stoll, in *Soft Nanoparticles for Biomedical Applications*, The Royal Society of Chemistry, 2014, pp. 342–371.

42. J. Shin, A. G. Cherstvy, and R. Metzler, *Phys. Rev. X*, 2014, **4**, 21002.

43. A. Moncho Jorda and I. Adroher-Benitez, *Soft Matter*, 2014, 5810-5823.

44. D. W. Yin, Q. L. Yan, and J. J. de Pablo, *J. Chem. Phys.*, 2005, **123**, 174909.

45. M. Quesada-Pérez, J. Ramos, J. Forcada, and A. Martín-Molina, *J. Chem. Phys.*, 2012, **136**, 244903–244909.

46. M. Quesada-Pérez, J. G. Ibarra-Armenta, and A. Martín-Molina, *J. Chem. Phys.*, 2011, **135**, 94109.

47. J. P. Valleau and L. K. Cohen, *J. Chem. Phys.*, 1980, **72**, 5935-5941.

48. P. M. Biesheuvel and M. van Soestbergen, *J. Colloid Interface Sci.*, 2007, **316**, 490–499.

49. J. N. Israelachvili, *Intermolecular and surface forces / Jacob N. Israelachvili*, Academic Press, London ; San Diego :, 1991.